ASTC Report: Atomistic and LLB models of HAMR

Lewis Atkinson, Matt Ellis, Roy Chantrell
Department of Physics, University of York, York, YO10 5DD, United Kingdom
(Dated: November 9, 2012)

I. ATOMISTIC SCALE MODELS OF MAGNETISATION DYNAMICS

A. Introduction

Work currently has been aimed at the development of a GPU accelerated code for more efficient simulation of the atomistic model. The model has then been used to simulate the linear reversal mode within iron platinum (FePt) systems, in particular looking into the effect of small particle sizes on this reversal.

Graphics Processing Units (GPUs) have become a popular device for the improvement of processing power in computing clusters. Currently GPU capable programs are developed using either CUDA or OpenCL library extensions. CUDA is developed by Nvidia whilst OpenCL is an open standard contributed by multiple groups. We have chosen to use CUDA rather than OpenCL since it is further developed with a better interface into the C/C++ languages. CUDA also has a set of libraries maintained by Nvidia which provide efficient GPU versions of commonly used tools; such as a Gaussian random number generator, FFT implementations and sparse BLAS functions.

The advantage of GPU acceleration is that the GPU device contains many compute cores that operate independently. This allows the program to launch threads onto these cores which execute the device code, known as a kernel, in parallel. However the limitations are that the memory which the kernels access must be allocated on the device. Therefore required data must be transferred onto and back off the device via the PCI-e bridge when needed for calculation on the device or output on the host. This has an associated latency which acts as a bottleneck in the program flow whenever a transfer is required, so to minimise this a transfer is only performed when the data is explicitly required.

The properties of FePt are of great interest for the further development of magnetic storage devices. FePt has a very large uniaxial anisotropy; this allows smaller grain sizes to be manufactured without compromising the long term storage stability of the device. *Ab initio* investigations by Mryasov *et al.*[1] showed that the exchange interactions between the atomic magnetic moments are long ranged and create the large anisotropy. This large interaction range implies that nanosized particles will have important differences with bulk systems.

The reversal mechanism is important for understanding the behaviour of the magnetic system during the write process. Usually the magnetization rotates towards the reversing applied field through the xy (transverse) plane in an circular or elliptical path. However it has also been shown to reverse via linear reversal at temperatures in the vicinity of the Curie point. The linear reversal mode is a path whereby the magnetization reverses by decreasing longitudinally instead and is much faster than the elliptical or cicular paths. This has been investigated by atomistic and micromagnetic models for bulk systems previously but the effects on these processess in nanometer sized finite grains, such as in a magnetic storage device, has not been investigated.

B. GPU Atomistic Code

The first section was the development of a GPU code for the simulation of atomistic scale magnetization dynamics. The atomistic spin model is highly suitable for GPU implementation, as the integration of the spin dynamics can be parallelised very easily. The spin dynamics model requires first the calculation of the local fields based at each of the atoms and then the calculation of the spin direction at the next timestep. The calculation of the local fields requires the knowledge of the total spin configuration of the system and cannot be completely separated to be calculated individually on different cores. This is still however calculated much faster on the GPU as parallel algorithms can be used. The calculation of the spin direction at the next time step is independent of the other spins once the local fields have been calculated and this section allows a great deal of parallelisation giving a large improvement over serial programs.

Since CUDA provides API for C++ the program was developed in a object orientated manner; this allows a simplified approach in which the important common functions are included within this and can be separated from the specific code for simulations. Using object inheritance this also allows different integration schemes to be implemented independently of each other and then utilised easily within separate simulation codes.

Whilst the standard CUDA API provides all the utilities for managing data and performing calculations with it on the GPU device there is also a set of libraries of common features that are used. The first is 'Thrust'; this takes the role of the Standard Template Library (STL) in C++ and provides useful algorithms, such as sorting, as well as higher level array functions that controls the data structures on the device memory. The second library is 'Cusp'; this provides a sparse amtrix storage classes and some sparse BLAS functionality which is used for the exchange interaction calculations. The 'Curand' library is also of important, this provides CUDA capable random number generators that are optimised for the GPU device allowing for efficient generation of random numbers which can be a major part of the model calculation.

As the spin information is simulated, the sections that only require information on a single atom can be easily parallelised and therefore this is ran concurrently on the GPU device. This is written in a CUDA kernel, this holds the instructions to be ran on the multiple cores on the device. Cruicial to the development of these kernels is the idea of 'warp divergence'; whilst a large subset of the data, known as a warp, can be processed at once the whole subset will always be waiting for the slowest amongst them with the faster ones idling while they wait. Therefore the kernel does not want to be written in such a way that one core will have many more instructions to do to limit this divergence.

The critical section of the model is the exchange interaction as this requires the data for the whole system and thus each spin must be at the same stage. The most efficient method for implementing the calculation of the exchange interaction is by representing the neighbour list as a sparse matrix; with the elements of the matrix representing the exchange strength between spins i and j. This can then be performed on the GPU and whilst the exchange calculation is relatively slow the data can be kept on the device before the next kernel is launched in parallel.

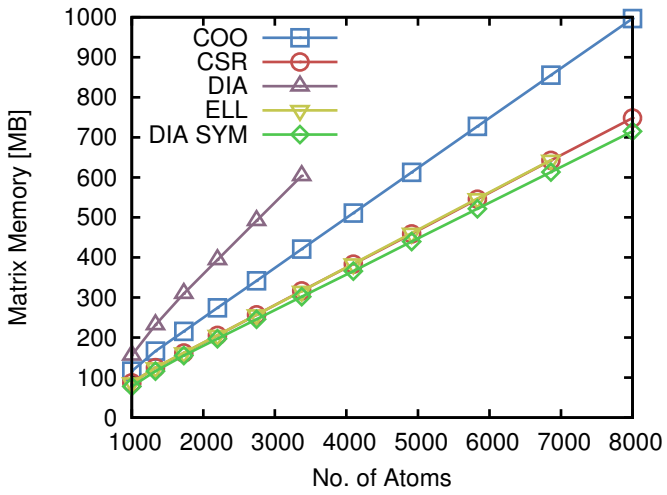

FIG. 1. The memory requirements for certain sparse matrix formats using CUSP for increasing system sizes. The system was based on an FePt Hamiltonian and as such had 1357 neighbours. The Diagonal format (DIA) has the worst memory requirements owing to sparsity pattern of the large number of neighbours, this could be improved with a better spin numbering system. The Coordinate format (COO) does not have an optimal storage method and even different numbering will not improve this. Both the Compresed Sparse Row (CSR) and Ellpack (ELL) formats provide near optimum storage as the indices are stored partly implicitly. The Symmetric Diagonal (DIA SYM) only has to store half of the matrix giving it the best memory efficiency. High memory efficiency is required due to the limited memory size on current GPUs, in this case 1280MB for the Nvidia GT570s.

Since the calculation of the exchange matrix is a bottleneck at each time step the choice of sparse matrix format is important. The Cusp library provides GPU capable sparse matrix functions in a variety of formats. The most general format is coordinate (COO) as this stores the row, column and values are stored explicitly in arrays and as such is easy to store and access but is not optimal in terms of memory size or multiplication speed. Other formats are compressed sparse row (CSR) or Ellpack (ELL) where the indices of one of the dimensions is stored implicitly by an array of offsets. ELL format is efficient for matrices that have a constant number of values per row which applies well to the exchange matrix as each atom has the same amount of neighbours. Diagonal (DIA) format also applies well to the exchange matrix as it is most efficient for matrices that have the non-zero values located along a certain number of diagonals which again is true for the exchange matrix. There is also another variant which utilises that symmetric nature of the exchange matrix. This Symmetric Diagonal (DIA SYM) format only stores the upper or lower half of the matrix and is

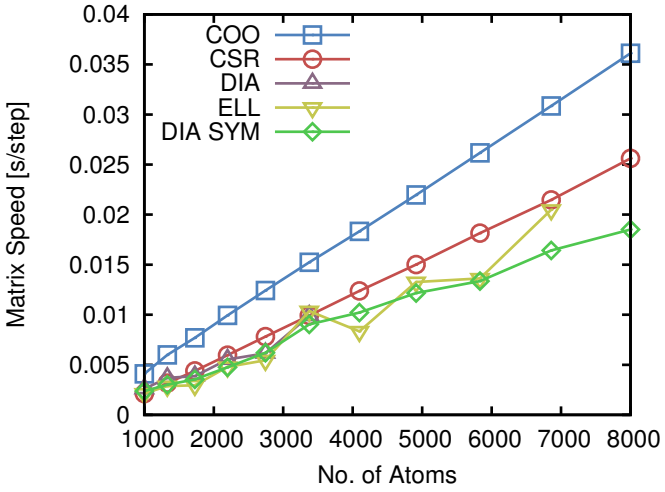

FIG. 2. The speed per time step for the atomistic model simulations using different matrix formats again for a FePt Hamiltonian. Since the matrix contains 1357 neighbours per spin this forms the dominant part of the run time. The COO and CSR formats are more general but this causes them to not perform as well as the other formats. The DIA, ELL and DIA SYM formats have very similar performance with little to differentiate between them though it appears that the ELL format for larger systems will not perform as well as the DIA formats. The speed was measured on the Nvidia GT 570 cards in the Wohlfarth cluster.

Figure 1 shows the calculated used memory for the different storage formats for a system with an FePt Hamiltonian, giving the spins 1357 neighbours. Since there is a large amount of interactions the sparsity pattern seems to favour the ELL format rather than the DIA format. This is due to the ELL format being more efficient for matrices with constant amounts of non-zeros per row, which due to the periodic boundary conditions is true in this case. The DIA format is more efficient with non-zeros populating the same diagonals, this can be affected by the numbering system and for the FePt case this creates a large amount of populated diagonals. The most efficient format is the DIA SYM, whilst the full DIA format is the least efficient by storing only the lower or upper half of the matrix the memory is used more effectively. The CSR format performs just as well as the ELL format owing to the similar nature of the storage of the values and pointers.

The performance of the matrix formats are shown in figure 2 for the same system as above. From this we can see that the more general formats don't perform as well as the others. The DIA, DIA SYM and ELL perform similarly show that these are the best choices for the exchange matrix. These formats perform the best as the memory that each thread is using is sequential in memory as thus has a small access stride compared to the other formats.

C. Finite Size Effects on Linear Reversal

The second section was the investigation of the linear reversal mode of FePt in finite sized systems. The long ranged FePt interactions lead to important finite size effects on the magnetisation and other properties, such as the uniaxial anisotropy. Recent *ab initio* work by Chepulskii *et al.*[2] on FePt nanoparticles comprising of only less than 100 atoms have very different properties to that of the bulk. Not only does the small nanoparticle size alter the magnetic anisotropy energy drop but the magnetic moment also drops. However these systems are on the 1nm scale which for FePt is smaller than the estimated stable grain size for magnetic media, 2.8-3.3nm. The results of Ref. 2 for cubic nanoparticles show a much reduced magnetic moment for a 14 atom cube whilst for a 63 atom cube the moment is much closer to its bulk value. The systems simulated are at a minimum 256 atoms (4 unit cells in each direction) which is much higher than the *ab initio* systems. Therefore utilising the bulk parameters to investigate the finite systems is only an approximation but should be applicable for reasonable system sizes.

The first stage was the simulation of reversal paths for a bulk FePt system using exchange parameters from *ab initio*, these results are shown in figure 3. The simulations were performed by starting the magnetisation in the positive z direction and then allowing the system to relax for 25 ps so that the equilibrium magnetisation is reached. After this an magnetic field of 10 T was applied in the negative z direction to make the magnetisation reverse. A 10 T field is rather large but was used to give reversal within a reasonable time scale for the test. The reversal path was simulated for a further 25 ps which in nearly all the cases the system had reversed. The figure shows that below the

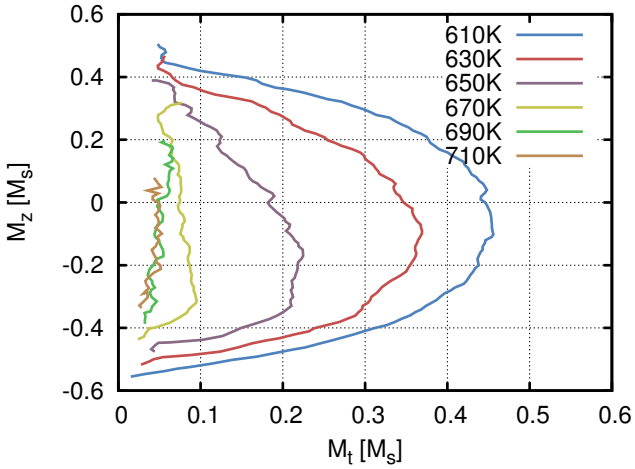

FIG. 3. Mean reversal paths for an example bulk FePt system with an applied field of 10T in the negative z direction simulated for 25 ps. At lower temperatures the reversal follows a elliptical path but nearer to the Curie temperature (700K) the reversal path becomes more linear with very small transverse magnetizations.

Curie temperature the mean reversal path is mostly circular, although there is a slight pull in the negative z direction due to the applied field re-magnetising the material. For this bulk system the Curie temperature is at about 700 K which is slightly lower than the experimental bulk results due to finite size effects. However independent of the actual Curie temperature the figure shows that as the temperature is near this point the linear reversal mode occurs. These results compare very well to those of Barker *et al.*[3] which also use a atomistic Langevin model to calculate the reversal modes.

To investigate the finite size effects first the magnetisation versus temperature phase diagram for a range of cubic grains has been calculated, shown in figure 4. As expected the smaller sized system show a reduction in the Curie temperature and above it there is still a remenant magnetisation due to the limited number of spins within the system.

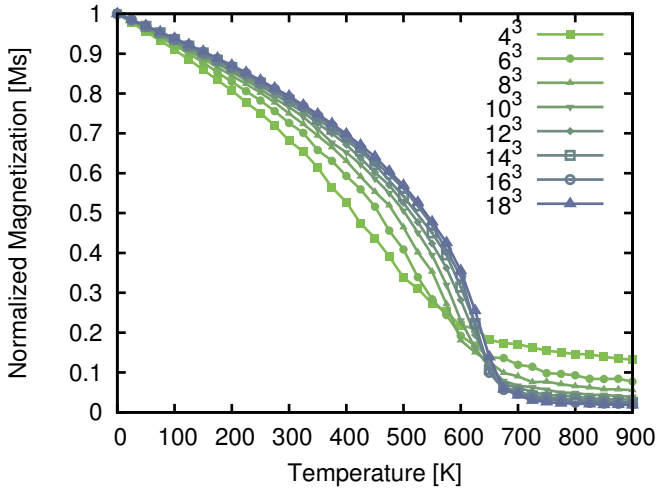

FIG. 4. Magnetisation versus temperature phase diagrams for a selection of finite grains. The sizes are represented in number of unit cells; therefore with a cell spacing of $a = 0.386$nm the sizes represent widths of 1.544nm, 2.316nm, ..., 6.948nm. The smallest three grain sizes are below the stable grain size diameter for FePt, 3.3-2.8nm. As the grain sizes is reduced the system cannot undergo a phase transition to the fully paramagnetic phase, while the Curie temperature drops lower. For a grain size of 4 unit cells the Curie temperature is about 400K and even above this temperature there is a much larger magnetization than larger grain sizes. For the larger grain sizes the system is acting more like a bulk system due to the number of atoms and also the dimensions being larger than the interaction range of the mediated exchange.

The reversal process in the finite grains has also been simulated by the same method for the bulk reversal results previously. Now since the Curie temperature has dropped the linear reversal regime has also dropped to a lower temperature. The systems still exhibit elliptical and circular reversal but again at a lower temperature as calculated for the bulk system. As shown in the magnetization temperature phase curves the smaller finite systems have a non-zero magnetization above the Curie temperature as a result of the small number of atoms. Therefore as the magnetization reverses the smaller grains have a larger transverse magnetization during reversal.

Figure 5 show the mean reversal paths at a selection of temperatures for finite systems with N = 6,8,10,12 unit cells per side. The bulk mean reversal paths shown in figure 3 show linear paths with transverse components of about $0.05M_s$ but the finite systems have a larger transverse component even at higher temperatures. This larger transverse component suggests that the magnetization is not as rigidly held towards the z axis by the anisotropy in these smaller systems. This is consistent with expecting that since the system size is smaller than the exchange interaction maximum range the two-ion anisotropy will have been weakened.

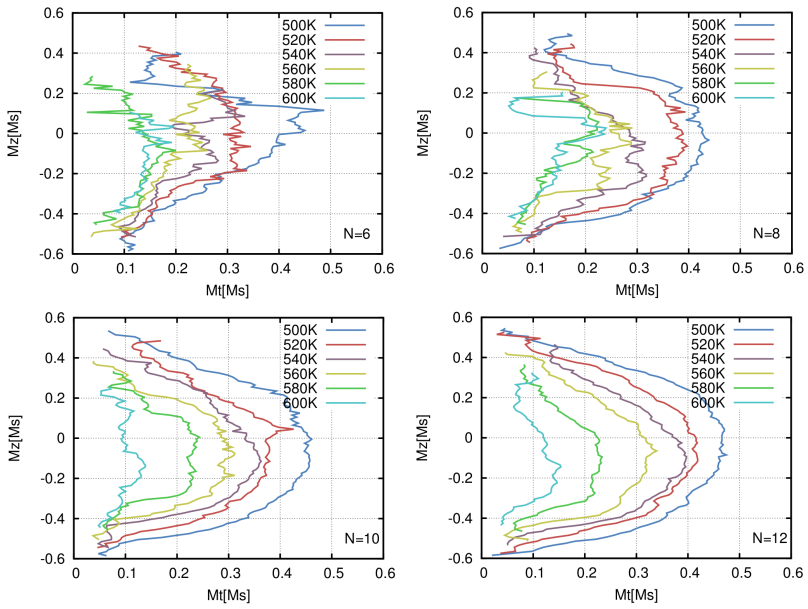

FIG. 5. A selection of mean reversal paths for finite subic systems, where N is the number of unit cells along each axis. The larger systems, N=10,12, behave in a similar manner to the bulk system but at a lower temperature due to reduction in the Curie temperature. The behaviour of the smaller systems , N=6,8, is different from the bulk system as now whilst the reversal is less elliptical there still exists a relatively large transverse component. This could arise from a weaker anisotropy allowing the magnetization to move away from the z axis.

Overall the reduction of the grain size has a clear effect on the reversal paths due to the truncation of the long range exchange interactions. However the effect of any form of surface anisotropy has not been taken into account yet. These extra surface interactions are considered in Ref. 2 to cause a large increase in the magnetic anisotropy energy for atomically thin slabs therefore even in the much large systems considered here this may conpensate the other finite size effects.

D. Conclusion

In conclusion, Nvidia's CUDA API has been used to develop an atomistic LLG model capable of running on a GPU device to improve the performance. The CUDA API allows for instructions to be performed over multiple data in parallel and as such is well suited for the spin dynamics model. Whilst many of the calculations can be performed in parallel the exchange interaction cannot and thus becomes an important section of the code. The exchange interaction is calculated from a matrix product and the storage format for matrix can be optimised to provide better memory storage and faster run time. The best formats appear to be the Ellpack and symmetric diagonal formats which have both efficient storage and runtime properties.

This GPU capable code has now been utilised to investigate the effects of finite systems on the reversal process in FePt. Bulk calculations show that near the Curie temperature the reversal happens in an linear way with little

transverse magnetization during the reversal. In the finite systems the Curie temperature drops and a full phase transition does not occur due to the limited size. This and a possbily weaker anisotropy is reflected in the reversal as now there is a larger transverse components even when the reversal path is mostly linear.

II. LLB MODELS OF THE HAMR PROCESS

A. Introduction

Magnetic data storage has shown exponential growth in both performance and utilisation since the technology was first established in the 1950's. The growth in performance was, in the main, achieved by reducing the size of the components used in the recording process. The exponential growth is currently being hindered by the physical constraints of the superparamagnetic limit, which is will halt growth entirely if a new approach for the technology can not be found. One approach to overcome the superparamagnetic limit is HAMR, which theoretically, would allow the continuation of the growth in performance of the technology.

The aim of the project is to investigate HAMR as a field cooled magnetisation process, using a simulated high anisotropy $L1_o$ FePt nano-granular thin film. The HAMR process is simplified to the reversing of the magnetisation of the thin film, using both an applied field and a heat assist.

B. Theoretical Model

The dynamical motion of the magnetization of the single grains is modeled as a single spin, using the Landau-Lifshitz-Bloch (LLB) equation. The LLB equation models the magnetisation m_i of a ferromagnetic nano particle on the sub pico-second time scale and at temperatures up to and above T_c, and is given as

$$\begin{aligned}\dot{\mathbf{m}}_\mathbf{i} = \gamma[\mathbf{m}_i \times \mathbf{H}_{\text{eff}}] + \frac{|\gamma|\alpha_{||}}{m_i^2}(\mathbf{m}_i \cdot \mathbf{H}_{\text{eff}})\mathbf{m}_i \\ - \frac{|\gamma|\alpha_\perp}{m_i^2}[\mathbf{m}_i \times [\mathbf{m}_i \times (\mathbf{H}_{\text{eff}} + \boldsymbol{\eta}_\perp)]] + \boldsymbol{\eta}_{||},\end{aligned} \tag{1}$$

where $\alpha_{||}$ is the longitudinal damping parameter and γ is the gyromagnetic ratio.

$$\alpha_\parallel = \lambda\frac{2T}{3Tc} \tag{2}$$

$\alpha_\perp$ is the transverse damping parameter

$$\alpha_\perp = \lambda(1 - \frac{T}{3Tc}) \tag{3}$$

Equation 2 applies only at or below T_c. Above T_c the damping constants are given by

$$\alpha_\parallel = \alpha_\perp = \lambda\frac{2T}{3Tc} \tag{4}$$

In order to introduce the effects of a non-zero temperature are introduced via a fluctuating magnetic field whose properties are determined by

$$\begin{aligned}\langle\eta_i^\mu\rangle &= 0, \\ \langle\eta_i^\perp(0)\eta_j^\perp(t)\rangle &= \frac{2k_\text{B}T(\alpha_\perp - \alpha_{||})}{|\gamma|M_\text{s}^0 V\alpha_\perp^2}\delta_{ij}\delta(t), \\ \langle\eta_i^{||}(0)\eta_j^{||}(t)\rangle &= \frac{2|\gamma|k_\text{B}T\alpha_{||}}{M_\text{s}^0 V}\delta_{ij}\delta(t), \\ \langle\eta_i^{||}\eta_j^\perp\rangle &= 0\end{aligned} \tag{5}$$

λ is the intrinsic damping constant which couples the spin system to the heat bath at the atomistic level, and H_{eff} is the sum of the applied, anisotropy, Zeeman and any interaction fields, which here includes the magnetostatic and exchange intergranular interactions.

The first term on the RHS describes the precession of the magnetic moment, the second term describes the damping of the magnitude of the magnetization and the third term describes the damping of the procession of the magnetic moment. The dynamics of the individual grains are calculated using a Heun scheme to numerically integrate the LLB equation. The parameters for the LLB equation ($M_s(T)$ and the longitudinal and transverse susceptibilities) are determined from atomistic calculations using a multiscale approach.

The model uses a voronoi construction to produce the granular microstruture. The voronoi construction produces a physically realistic picture of the film, including a grain size dispersion and some microstructural disorder. The model generates three dimensional grains 5 - 10nm in diameter and height, each assumed magnetically to behave as a single domain. The easy axis for each of the grains is aligned with the z-axis. The Voronoi construction produces a film with a dispersion of grain size which is approximately lognormal. The standard deviation σ_V can be varied by changing the degree of randomness of the seed points for the Voronoi construction. Here we studied a system with $\sigma_V \sim 0.35$. The local field acting on a grain is calculated as follows

$$\begin{aligned}\mathbf{H}_{eff} = \mathbf{H}_{applied} + \sum_{ij} \frac{\mu_j}{r_{ij}^3}(3(\hat{r}_{ij}\cdot\hat{\mu}_j)\hat{r}_{ij} - \hat{\mu}_j) \\ + H_e^{ij} + \frac{H_k}{2}(\hat{e}\cdot\hat{\mu})\hat{e}\end{aligned} \tag{6}$$

where $\mathbf{H}_{applied}$ is the (uniform) external applied field. The second term on the RHS of Equn. 6 is the magnetostatic term, which is calculated as a direct pairwise summation within a cut-off radius of 8 grain diameters, with long-range effects introduced via a mean field. The remaining terms in Equn. 6 are the contributions from the exchange and anisotropy. The intergranular exchange interaction is formulated under the assumption that the exchange energy is proportional to the contact area between neighboring grains. The approach also allows for a dispersion in the exchange J_{ij} due to variations in grain boundary thickness and composition. In terms of reduced parameters (relative to the median values L_m, A_m, J_m)

$$H_e^{ij} = H_{exch}\left(\frac{J_{ij}}{J_m}\right)\left(\frac{L_{ij}}{L_m}\right)\left(\frac{A_m}{A_i}\right)\hat{s}_j, \tag{7}$$

where $H_{exch} = J_m L_m/(a^2 M_s A_m)$. In practice H_{exch} is set by the requirement that the average exchange at saturation has a certain value H_{exch}^{sat}, that is

$$H_{exch}^{sat} = N^{-1} H_{exch} \sum_i^N \sum_{j\in n.n}\left(\frac{J_{ij}}{J_m}\right)\left(\frac{L_{ij}}{L_m}\right)\left(\frac{A_m}{A_i}\right), \tag{8}$$

The temperature of the system is assumed spatially uniform. The temperature increase associated with the laser pulse is modeled as a step change from ambient temperature (300K) to the maximum temperature. The temperature then returns to ambient following a Gaussian form in a characteristic time, set to 0.5ns throughout the investigation. With this cooling rate the system temperature returns to ambient in $\sim$ 1.2ns. All temperatures stated in the results section are given as the maximum temperature during the HAMR simulation. The anisotropy of the individual grains are modeled as percentage of the bulk magnetocrystalline anisotropy constant, K_v, of $L1_o$ ordered FePt. This models a system in which each grain is partially $L1_o$ ordered, giving an anisotropy equal to a percentage of $L1_o$ ordered FePt. Each grain within the thin film has an equal K_v.

C. Temperature Profile

To simulate the temperature rise associated with the HAMR process, the temperature is modeled as a step change form ambient (300K) to a maximum then following a Gaussian back to ambient in a characteristic cooling time. Figure 7 shows the temperature profile of the system over a range of maximum temperatures from ambient (300K) to T_c (660K). The characteristic cooling time, of 0.5ns, returns the system temperature to ambient within 1.0ns after the temperature rise.

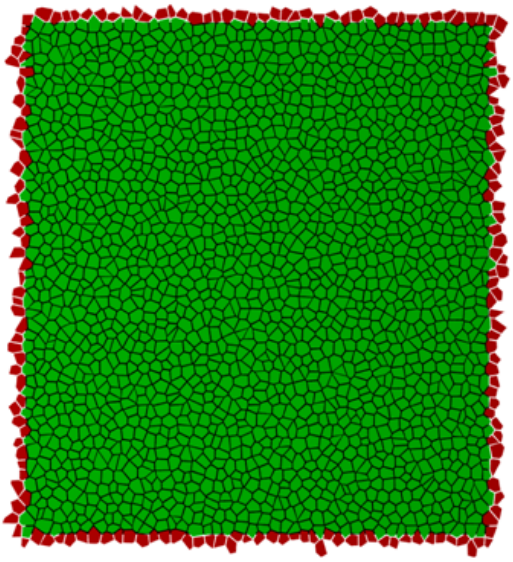

FIG. 6. A plan view of the granular thin film produced by the voronoi construction. The modeled thin film shows microstructural disorder and grain size dispersion. The thin film contains approximately 80 × 80 6nm grains.

III. RESULTS

A. Thin Film Reversal process

The initial study concentrated on the 20% $L1_o$ ordered case as this give the minimum anisotropy required to ensure stability of the magnetisation for 6nm grains. Figure 8 shows hysteresis curves as function of temperature. As expected, the coercivity decreases with temperature. The loops also indicate a reduction of the effect of interactions with increasing T, as follows. At low temperatures the loops exhibit a change of slope in negative fields. This is usually interpreted as arising from the effects of exchange and magnetostatic interactions which drive the system into low energy states with low magnetization which are relatively stable and slow the approach to negative saturation. It can be seen in Figure 8 that this effect is reduced with increasing temperature, and is not present at the highest temperatures investigated. This suggests that the intergranular interactions are not a significant contribution to the high temperature magnetization process.

The reduction of the effect of interactions at elevated temperatures is shown in Fig. 9, which shows the reversal field (defined as the field required to reverse 95% of the film magnetization) as a function of the Intergranular Exchange field (IGE) for various temperatures. The variation becomes less pronounced with increasing temperature, suggesting that effect of the exchange field on the magnetization process decreased with increasing temperature.

B. Dynamics of the HAMR process

HAMR is essentially a Field-Cooled Magnetization (FCM) process, albeit at extreme rates of temperature reduction. A further complication is the presence of rapidly varying magnetic fields, although for simplicity this study considers time-independent applied fields. Here we lead to a description of HAMR as a FCM process, proceeding with a study of the time dependence of the magnetization through the HAMR process. Figure 10 shows the M_z time sequence for the simulation with a 12000Oe reversing field, for the 20% $L1_o$ ordered case. At temperatures well below T_c one can distinguish three time regimes. There is an initial very rapid reduction of the magnetization, driven by the rapid temperature increase This involves longitudinal magnetization changes; the reduction in the magnitude of the magnetization of the grains. The longitudinal relaxation time is of the order of a few hundred fs, as a result of

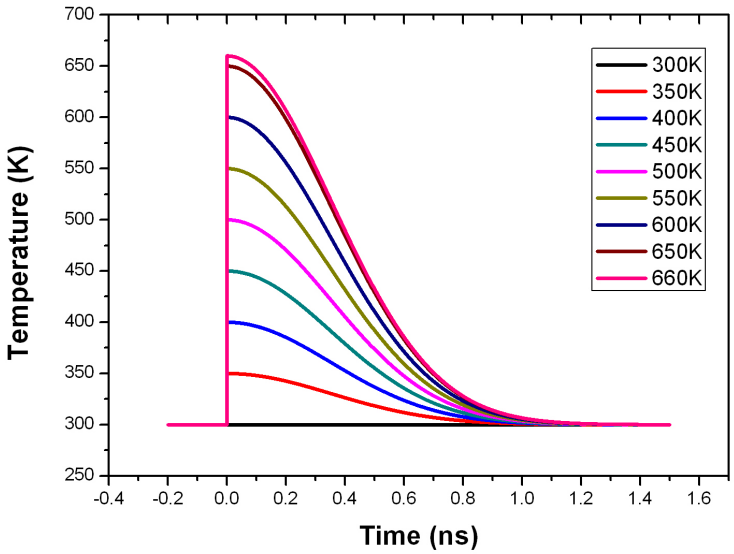

FIG. 7. The temperature profile used to represent the HAMR style heat and subsequent cooling. The temperature profile is shown over a range of maximum temperatures from the ambient constant temperature case (300K) up to T_c.

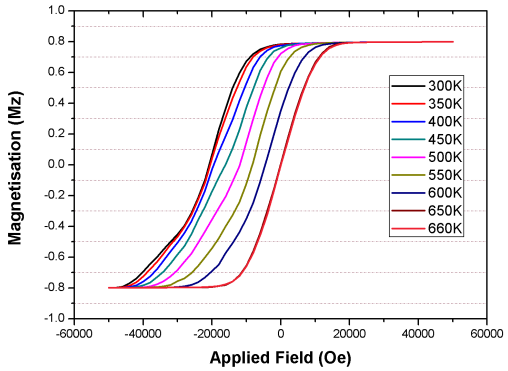

FIG. 8. Hysteresis curves as a function of temperature for an anisotropy value of 20% of fully ordered $L1_o$ FePt. At low temperatures the change of slope in negative fields is indicative of intergranular interactions, whose effect decreases with increasing temperature.

which the magnetization very rapidly follows the temperature increase. After this process magnetization proceeds by precessional switching over the (reduced) energy barriers. Finally, as the temperature lowers there is a slower change in the magnetization caused by thermally activated reversal events which, depending on the grain size, can be significant out to 10-20 ns. The heat assist effect is clear from the data presented. At ambient temperature the field is insufficient to reverse a significant number of grains. As the temperature increases increasing numbers of grains can be switched due to the reduction in the value of K. The HAMR process is illustrated in Fig. 11 which shows the fraction of the grain size distribution reversed at each temperature. Fig. 11 demonstrates that the smaller grains are reversed at low temperatures, with an increasing fraction of large grains reversed at elevated temperatures. In the highest temperature simulations the mean volume is marginally increased, as a portion of the relatively smaller grains are in the initial orientation after the simulation. This is consistent with the recent introduction of the concept of the 'thermal writability' which defines the requirement that the write field H_{wr} should be sufficiently large not only to switch the magnetization but also to ensure that at the freezing temperature (T_f) of the grain $M_s(T)VH_{wr}/kT_f$ is large enough to ensure that there is no thermally-induced back-switching of the magnetization.

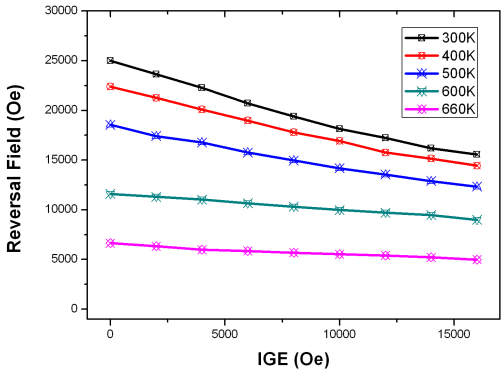

FIG. 9. Dependence of the reversal field on the Intergranular Exchange field (IGE) as a function of temperature for an anisotropy value of 20% of fully ordered $L1_o$ FePt.

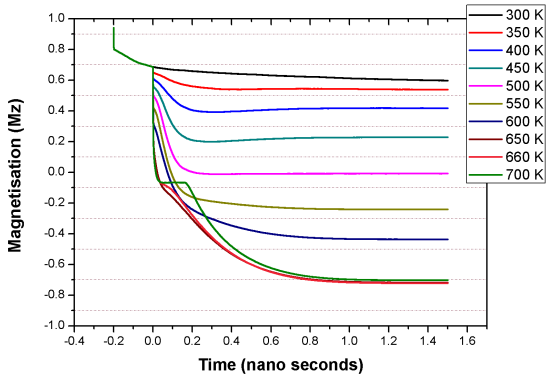

FIG. 10. An M_z time sequence of the whole system, for 20% $L1_o$ grains, showing the effect of increased temperature, during the HAMR simulations.

This supports the conventional picture of HAMR as a process driven by thermal activation over thermally reduced energy barriers, and applies to all peak temperatures considered up to 600K. However, it is important to note that in these processes the magnetization is not completely reversed. Complete reversal is observed only for temperatures $T \geq 650$K. This effect is even more pronounced in calculations for 100% ordered FePt, as shown in Fig. 12, where reversal is not seen even for temperatures as high as 640K. It is also interesting to note that there is a significant change in behavior between temperatures of 640K and 660K. This can be interpreted as arising from the onset of the linear reversal process [3], which is characterized by ultrafast reversal via longitudinal magnetization changes. The transition to linear reversal is demonstrated in Fig. 13, which plots time averaged longitudinal vs transverse magnetization throughout the HAMR process for the 20% $L1_o$ ordered case. The results are consistent with the atomistic simulations given in [3]. At low temperatures the reversal is by coherent rotation, characterized by a constant magnitude of the magnetization throughout the process, with the magnetization magnitude decreasing with increasing temperature. In this regime the reversal is precessional with characteristic switching times in the order of 10-100ps. At a temperature of 650K, however, reversal proceeds via a different, non-precessional, switching mechanism termed linear reversal. While reversal proceeds by precession of individual spins at the atomistic level, the macroscopic spin associated with individual grains reverses via collapse of the magnetization through zero.

This mechanism is extremely fast with characteristic times of the order of the longitudinal relaxation time (100fs). This is illustrated in Fig.14 which shows M_z vs T for a peak temperature of temperature if T_c and a range of cooling rates. The magnetization vanishes and reverses rapidly and essentially follows the time evolution of the temperature during the cooling process.

In terms of applications in recording, the final state of the system after the HAMR process is of central importance. Here we charcaterize the state in terms of a reversal probability, taken as the reduced magnetization (relative to

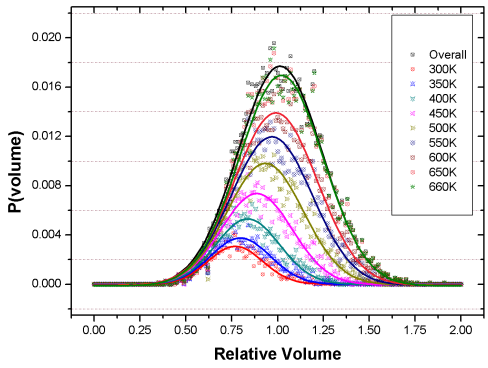

FIG. 11. The spread of the relative volume of the FePt grains within the thin film, showing the spread of the volume for the grains which have reversed their magnetization over a range of maximum system temperatures during the HAMR process.

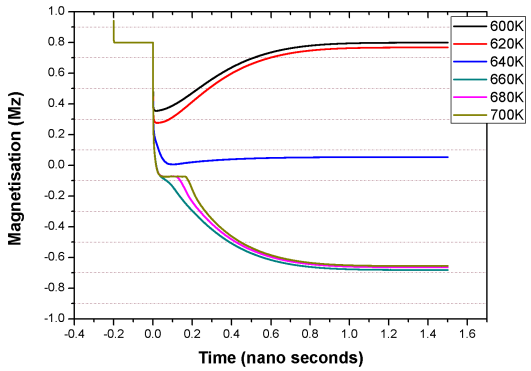

FIG. 12. An M_z time sequence of the whole system, for 100% $L1_o$ grains, showing the effect of increased temperature, during the HAMR simulations. Note the reduced temperature scale in relation to Fig. 10

saturation), after the HAMR process. Figure 15 shows the reversal probability over a range of anisotropy values and maximum system temperatures. This clearly shows the increase in the temperature required to initiate the reversal process in the higher anisotropy simulations. Above an anisotropy of 60% $L1_o$ ordered grains and below a temperature of 600K the system shows very low or zero magnetisation reversal. The data also show that, when the maximum system temperature reaches T_c, reversal is achieved for all anisotropy values. For relatively low anisotropy values it can be seen that there is a relatively weak dependence of the reversal probability, although the probability does increase up to T_c. There is a much more dramatic effect of temperature for values on anisotropy approaching that of Bulk FePt. Here, peak temperatures as high as 640K are not sufficient to cause switching of the magnetization; a switching path is only available via linear reversal, which suggests that this mechanism will become increasingly the dominant process as the anisotropy value increases in line with the requirement of thermal stability at ultra-high densities.

These two constraints; the higher anisotropy regimes needing increasingly higher temperatures (approaching T_c) to initiate reversal, means that the temperature range where reversal is seen is reduced as the anisotropy is raised. This is a significant result for HAMR, as a narrower range of temperature where magnetization reversal is seen means the reversal process must take place over a smaller timescale, leading to the possibility of incomplete switching. In this respect, the intrinsically fast (ps timescale) of switching via linear reversal could be an important factor.

[1] O. N. Mryasov, U. Nowak, R. W. Chantrell, and K. Y. Guslienko, Europhysics Letters **69**, 805 (2005).
[2] R. V. Chepulskii and W. H. Butler, Applied Physics Letters **100**, 142405 (2012).

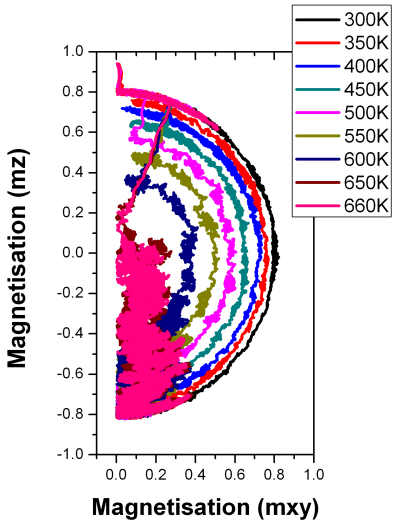

FIG. 13. The reversal of the individual grains magnetisation for the 20% $L1_o$ ordered case, over a range of maximum system temperatures. The applied field is 6kOe.

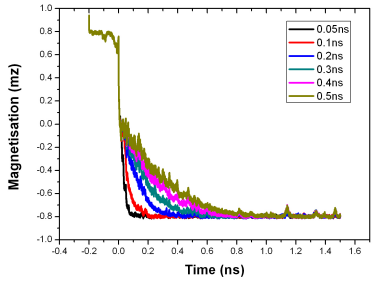

FIG. 14. Switching via linear reversal for a single grain, over a range of cooling rates. The maximum temperature if T_c and the applied field is 6kOe.

[3] J. Barker, R. F. L. Evans, R. W. Chantrell, D. Hinzke, and U. Nowak, Applied Physics Letters **97**, 192504 (2010).

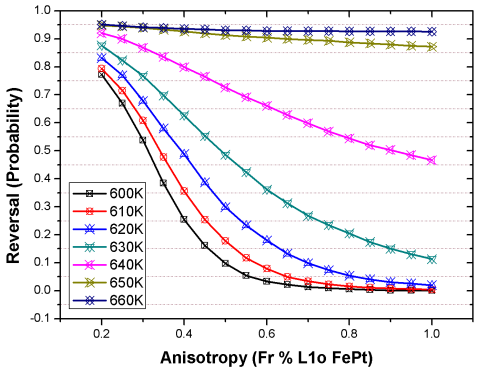

FIG. 15. The reversal probability of the whole system with a 12000Oe applied field, over a range of maximum system temperatures (600K - T_c) and anisotropies (20% - 100% $L1_o$ ordered FePt grains).